High-momentum components and temperature dependence of the Compton profile of beryllium

S. Huotari,* K. Hämäläinen, and S. Manninen
Division of X-Ray Physics, Department of Physical Sciences, P.O. Box 64, FIN-00014 University of Helsinki, Finland

C. Sternemann, A. Kaprolat, and W. Schülke
Institute of Physics, University of Dortmund, D-44221 Dortmund, Germany

T. Buslaps
European Synchrotron Radiation Facility, BP 220, F-38043 Grenoble Cedex, France
(Received 30 November 2001; published 5 August 2002)

We present Compton-scattering studies on the high-momentum components of the valence electron momentum density in beryllium. The experiments were performed with incident photon energies of 29 and 56 keV with a momentum space resolution of 0.10 and 0.16 a.u. units of momentum, respectively. The temperature dependence of the Compton profile and the high-momentum components were studied within the temperature range of 40–850 K. The incident photon energy was 56 keV and the photon scattering vector was along the [110] reciprocal lattice vector. We compare the temperature dependence of the experimental Compton profiles to empirical local pseudopotential computations that take into account both thermal expansion and disorder. The position and intensity dependence of the high-momentum components as a function of temperature in solid beryllium were found to be quite small, which suggests that the valence electron wave functions in beryllium are not significantly affected by thermal disorder. This proves that the previously observed broadening of experimental Compton profiles in comparison to highly accurate theoretical profiles is not due to thermal disorder, and other reasons, e.g., correlation, need to be sought as the source of the broadening.

DOI: 10.1103/PhysRevB.66.085104 PACS number(s): 71.18.+y, 78.70.−g, 71.15.−m

I. INTRODUCTION

It has recently been shown that Compton scattering of high-energy x rays from a synchrotron radiation source is a very useful tool in studying the electron momentum densities in many materials.[1–14] The quantity measured in these experiments is the double-differential cross section for photon scattering, which is directly related to the so-called Compton profile $J(p_z)$. The Compton profile, in turn, is related to the momentum density $N(\mathbf{p})$ of the electrons in the system under study by being the integral of $N(\mathbf{p})$ over two dimensions p_x and p_y. The direction of p_z is determined by the scattering vector $\mathbf{q}=\mathbf{k}_2-\mathbf{k}_1$, where $\mathbf{k}_1$ and $\mathbf{k}_2$ are the wave vectors of incoming and scattered photons, respectively. The Compton profile gives unique information on the electron wave functions and the related electronic structure. Furthermore, the high-resolution measurements reveal valuable details in (i) the structure of the Fermi surface, for the purposes of e.g., materials science, (ii) the electron-electron correlation, an important issue in many-body physics, as well as (iii) the wave-function modulation by the periodic lattice potential, yielding information on the lattice potential itself and, for example, thermal disorder of the ionic lattice. This modulation, i.e., the interaction between the valence electrons and the ions, can be seen in the electron momentum density first in the structure of the Fermi surface, and second, as the so-called high-momentum components of the wave functions and thus also of the momentum density. Despite the fact that these high-momentum components have been well understood as a result of the valence electron wave functions being Bloch waves, the experimental studies of their structure has been very scarce, because their contribution to the momentum density of metals is quite weak. To the authors' knowledge, the only direct observation was made by Oberli *et al.* using positron annihilation.[15,16] Schülke *et al.*[5] measured a total of 11 directional Compton profiles of Li and reconstructed the three-dimensional electron momentum density, finding signatures of the high-momentum components. Furthermore, Sternemann *et al.*[9] measured Compton profiles of Li at room temperature and at 95 K, finding also signatures of the high-momentum components in the difference of the Compton profiles between the two temperatures. However, to date, no direct observation of the high-momentum components in a Compton profile has been reported.

Compton scattering itself is a quite unique tool in physics, since while practically all other spectroscopical tools probe transitions between electronic levels, Compton scattering gives direct information of the wave functions of occupied electron states. The studies are performed in momentum space, but as the high-momentum components originate from the periodic lattice potential, their study, in turn, gives information on the properties of the wave functions and the potential in position space. This way the study of Compton profiles serves as an exceptional link between the momentum space and the position space properties of the electron gas, the ion lattice, and their mutual interaction.

There are also other methods to study the Fermi surface, such as the de Haas–van Alphen (dHvA) method and positron annihilation (angular correlation of annihilation radiation). However, the dHvA method requires a low sample temperature and therefore is not well suited for studying finite-temperature effects on the Fermi surface. Both methods are moreover limited by a high sensitivity of sample (especially surface) purity. Compton scattering is not limited

by any of these conditions, and is well suited for temperature- or pressure-dependent studies.[9,10]

A finite temperature has several effects on the electron momentum density. First of all, the crystal lattice expansion corresponds to a shrinkage of the reciprocal lattice, which means that the electrons at a finite temperature will be confined to states with a smaller momentum than they are at $T=0$ K. Second, the vibration of the ions in the crystal around their equilibrium positions effectively smears out the lattice potential. This thermal disorder has been treated in two different ways in literature. One way is to calculate the electronic properties of a frozen but disordered system with the ionic positions in randomly disordered positions and to average the different configurations.[17] The other possibility is to regard the ions to stay perfectly ordered at their equilibrium positions, and incorporate thermal disorder in their potential. This can be done, for example, within the pseudopotential approximation by means of a plane-wave expansion of the valence electron wave functions. Finite temperature effects are then considered by multiplying the plane-wave components of the pseudopotential by the appropriate Debye-Waller factors as to simulate thermal disorder.[18] A third factor is the finite-temperature deviation of the Fermi-Dirac occupation number function from the zero-temperature step function. Since the Fermi temperature (typically 10 000 K) of a metal is much higher than its melting point, this effect is negligible in solid metals when Compton profiles are concerned.

Although the basic theory of Compton scattering is well known, some unexplained differences between theoretical and experimental results have emerged lately,[1,4,5,19] mostly due to enhanced experimental accuracy. These differences include (a) broader Compton profiles in experiment than anticipated by accurate one-electron calculations, (b) apparent washing out of the sharp Fermi-surface related structures, and (c) asymmetry of the Compton profiles. Partial explanation for all these have very recently been suggested to originate from final-state effects, i.e., the interactions between the electron and the hole, and between the ejected electron and the electron gas.[19,20] Today these effects are understood to explain the differences between experimental and theoretical Compton profiles, when the experiments are performed with a low incident photon energy (order of 10 keV or less). The final-state effects concerning (a) and (b) should in principle disappear when the incident photon energy exceeds 20 keV, but similar effects have been seen also with high incident photon energies (high-precision studies have been made at least with energies up to 60 keV).[1,21] Asymmetry of the core-electron related Compton profiles is understood to remain visible even with these high photon energies, but the presence of the broadening effects still waits for explanation. These effects can most likely be due only to ground-state effects of the electron gas, but understanding them completely would require at least two advances in the computational methods for the inhomogeneous (and possibly even highly correlated) electron systems, namely, the possibilities to account for correlation effects and thermal disorder. Correlation is well understood in the case of homogeneous electron gas, of which conduction electrons of the alkali metals are a good approximation. Up to date, the correlation effects in Compton-scattering data analysis are taken into account by assuming the electron gas to be homogeneous, which leads to the so-called Lam-Platzman correction to the Compton profiles.[22] However, it has been shown that in an inhomogeneous electron gas with a complicated Fermi surface, such as Be, the Lam-Platzman correction is not adequate to explain the differences between experimental and theoretical Compton profiles.[1] On the other hand, quantum Monte Carlo calculations[23] have suggested that correlation would not be the only reason for the differences between theoretical and experimental Compton profiles, at least in the case of Li. It was recently suggested that some of this broadening could also be explained by thermal disorder in the electron-gas ground state.[17] Unfortunately the state-of-the-art computational schemes utilizing the local-density approximation cannot account for thermal disorder. This work is a part in a systematic series of experimental and computational studies for understanding all the above-mentioned effects and attempting to fill the gap between experimental and theoretical Compton-scattering results.

Since the suggestion of thermal disorder being partly behind the broadening of Compton profiles, studies of the Compton spectra as a function of temperature have been performed with Li and Al.[9,24,25] The results have not supported the suggested picture, as it has turned out that lattice expansion has a greater effect on the electron momentum density than thermal disorder has, and furthermore, even thermal disorder has an effect that is opposite to the results of the above-mentioned model. This, however, does not necessarily imply that the fine structure in the derivatives of the Compton profiles could not be washed out by thermal disorder.

While the previous studies on the temperature dependence of Compton profiles were performed on metals with the valence electrons obeying the homogeneous electron-gas approximation, we have expanded these studies to a system with an inhomogeneous valence electron gas. Thus, in order to systematically study the above-mentioned differences between experimental and theoretical results, we have tried to separate the effect of thermal disorder from correlation effects in a inhomogenous electron gas. Bearing this purpose in mind, we have conducted experimental studies on Compton profiles of single crystalline Be at various temperatures ranging from 40 to 850 K and calculated the Compton profiles at the corresponding temperatures by using an empirical local pseudopotential method.

II. THEORY

The momentum density $N(\mathbf{p})$ of an electron system is the absolute square of its wave function in momentum space. If the electron is specified by a band index ν, then

$$N(\mathbf{p})=\sum_{\mathbf{k},\nu}\left|\int d\mathbf{r}\,\psi_{\mathbf{k},\nu}(\mathbf{r})e^{i\mathbf{p}\cdot\mathbf{r}/\hbar}\right|^2, \tag{1}$$

where the summation is over the occupied states.

In a limit of independent electrons, it is possible to expand the wave functions of the valence electrons in plane waves,

$$\psi_{\mathbf{k},\nu}(\mathbf{r}) = \sum_{\mathbf{G}} a_\nu(\mathbf{k}+\mathbf{G}) e^{i(\mathbf{k}+\mathbf{G})\cdot\mathbf{r}}. \quad (2)$$

The electron momentum density can then be written as[26]

$$N(\mathbf{p}) = \sum_{\mathbf{k},\nu,\mathbf{G}} |a_\nu(\mathbf{k}+\mathbf{G})|^2 \; n_\nu(\mathbf{k}) \delta_{\mathbf{k}+\mathbf{G},\mathbf{p}/\hbar}. \quad (3)$$

Here $\mathbf{k}$ is a wave vector in the first Brillouin zone and $\mathbf{G}$ a reciprocal lattice vector. The Fermi-Dirac occupation number function for a state $\mathbf{k}$ in a band ν is written as $n_\nu(\mathbf{k})$, and is equal to unity for occupied electron states below the Fermi energy, and zero elsewhere. The three-dimensional momentum density has thus contributions centered around reciprocal lattice vectors $\mathbf{G}$. The magnitude, shape, and position of these high-momentum components carry information on the underlying crystal structure and the strength of the electron-ion interaction. The Compton profile, which is the measurable quantity, is then the projection of $N(\mathbf{p})$ onto the scattering vector, whose direction is that of the p_z axis, and can be identified as

$$J(p_z) = \int_{-\infty}^{\infty}\int_{-\infty}^{\infty} N(\mathbf{p}) dp_x dp_y. \quad (4)$$

It is possible to estimate the effect of thermal disorder on the wave functions by using a plane-wave basis set within the pseudopotential method.[27] In this picture the local pseudopotential $v_{\text{pseudo}}(\mathbf{r})$ is considered in the plane-wave expansion

$$v_{\text{pseudo}}(\mathbf{r}) = \sum_{\mathbf{G}} V(\mathbf{G}) e^{i\mathbf{G}\cdot\mathbf{r}}. \quad (5)$$

The temperature effect is then taken into account by multiplying the potential coefficients $V(\mathbf{G})$ by the corresponding Debye-Waller factors

$$W(T,\mathbf{G}) = \exp\left(-\frac{B(T)|\mathbf{G}|^2}{16\pi^2}\right), \quad (6)$$

where $B(T)$ is the Debye parameter.[18] This method was used succesfully in Ref. 9. We calculated the momentum density of Be using an empirical method, i.e., by fitting the coefficients $V(\mathbf{G})$ to minimize the difference between the experimental and calculated Compton profiles. The following coefficients were found to give a reasonable agreement: $V(100)=0.03$, $V(002)=0.2$, $V(101)=0.15$, $V(102)=0.05$, and $V(110)=0.3$ a.u.

The directional Compton profile differences of Be are mainly influenced by the shape of the occupied region in the extended zone scheme determined by the energy eigenvalue spectrum. Therefore, only taking into account the potential coefficients that reproduce the shape of the directional Compton profiles within $k<k_F$, results in pseudo wave functions that do not properly fulfill the condition that the valence electron wave functions need to be orthogonal to the core-electron wave functions. The true wave functions, which are responsible for high-momentum components, evidently have to include the core orthogonalization. For that reason, the values of the potential coefficients above have to be considered as a lower limit, when used to account for the high-momentum components and their temperature dependence. On the other hand, the pseudopotential coefficient corresponding to the $\mathbf{G}=[110]$ reciprocal lattice vector, namely $V(110)$, was fitted to reproduce the high-momentum component peaks, whose height sensitively depend on the value of $V(110)$ thus reflecting its origin from a $\mathbf{G}_{110}$ Bragg reflection. This finds verification by the fact that this high-momentum structure has its onset nearly at $p_z=|\mathbf{G}_{110}|-k_F$, where k_F is the free-electron Fermi momentum. It turned out that the value of $V(110)$ does not significantly influence the overall shape of the Be Compton profiles. Since $V(110)$ was fitted to features of the true wave function, it may not be surprising that its value is larger than those of the other coefficients. It is noteworthy that in a study[28] that employed a similar method for calculating the dynamic structure factor $S(q,\omega)$ of Be for small energy transfer values, the value of $V(110)=0.15$ was obtained in a fit to a double peak structure originating from the $V(110)$ excitation gap in the band structure. This value is comparable to the largest coefficients of the fit described above.

The eigenvalue problem was solved with a grid of 0.01 a.u. in the momentum range of 0–4 a.u. in each direction; this is equivalent of 2.1×10^5 points within the irreducible part of the Brillouin zone. The well-known features of the Fermi surface, namely, the holelike coronet and the electronlike cigars, were reproduced by this pseudopotential. The Debye-Waller factors were obtained from Ref. 29 and the lattice constants from Ref. 30. The electron-electron correlation in the ground state of Be valence electrons was taken into account by using the isotropic Lam-Platzman correction taken from Ref. 1. This correlation correction, however, does not have any temperature dependence.

Finally, as we studied the derivatives of the computed Compton profiles, we can conclude that, at least in the case of Be, the fine structure of the derivatives of the Compton profiles (see the analysis in Ref. 1) is not washed out even when thermal disorder is taken into account within the calculation.

III. EXPERIMENT

The experiments were accomplished at the European Synchrotron Radiation Facility (ESRF) beam line ID15B. The experimental details are similar to those described in Ref. 1. Synchrotron radiation from an asymmetric multipole wiggler was monochromatized ($E_1=29$ and 56 keV) and horizontally focused to a size of 300 μm (H)$\times$5 mm (V). The Be single crystal sample was a 10-mm-long stick with a rectangular (1×1 mm^2) cross section. The spectra of Compton scattered photons were recorded using a scanning crystal spectrometer,[31] which had a resolution of 0.10 a.u. of momentum for $E_1=29$ keV and 0.16 a.u. for $E_1=56$ keV. Typical count rates were about 4000 cps at the Compton peak. At each temperature, a total of 10^6 counts were col-

lected at the Compton peak. The incident photon intensity was monitored using a Si *pin* diode.

The spectra were corrected for sample and air absorption, spectrometer efficiency, dead time, an almost negligible linear background, and core asymmetry as described in detail in Ref. 21. The temperature was controlled by a closed cycle liquid-He cryostat with a temperature controller (the lowest sample temperature was 40 ± 10 K) and for the higher temperatures by an oven environment (sample temperatures 650 ± 20 and 850 ± 50 K), similar to the one used in Ref. 9. The temperature was measured using two independent sensors. A Pt-100 sensor was attached to the sample mount and a thermocouple was attached to the tip of the stick-shaped sample using a ceramic Cerastil *C*-3 glue. The same ceramic glue was also used to attach the sample itself to the heater. During the experiment, the temperature reading at the thermocouple attached to the end of the sample was always slightly closer to room temperature than the temperature reading at the cold finger or the heater base. The reason for this is the radiative cooling/heating combined with the finite thermal conductivity of the sample, since the sample was heated/cooled at one end only. While the sample was positioned so that the beam spot was located at the geometrical center of the sample, the actual temperature at the illuminated spot was estimated to be the average of these two readings. The uncertainty of the temperature was estimated by assuming that the temperature variation was linear along the sample.

The Compton profiles were recorded at room temperature in both environments to ensure the comparability of the low- and high-temperature data. Both room-temperature profiles were found to be identical within the statistical accuracy.

IV. RESULTS AND DISCUSSION

One typical example of our experimental results is shown in Fig. 1, where we present the $\mathbf{q}\|[110]$ room temperature valence Compton profile of Be obtained with incident photon energies of 29 keV and 56 keV, together with the corresponding theoretical Compton profile calculated with the empirical pseudopotential method, including the Lam-Platzman correction to account for correlation. The Compton profile contribution of the tightly bound core electrons was taken from Ref. 1 and subtracted from the data to obtain the valence electron Compton profiles.

The top panel represents the total valence profile at an incident photon energy of 56 keV, and the middle panel a vertical closeup of the bottom of the same profile. The bottom panel is similar to the middle panel but for an incident photon energy of 29 keV. The missing points around 3 a.u. in the 56-keV data are due to a glitch of the analyzer crystal at this energy, i.e., the analyzer crystal has another simultaneous reflection at the corresponding Bragg angle. The theoretical profiles are broadened to reflect the experimental resolution by convoluting them with a Gaussian possessing the full width at half maximum (FWHM) of the experimental resolution function. As the general shape of the profile is considered, it can be seen that the experimental profile is somewhat lower at small $|p_z|$ and higher at high $|p_z|$, in comparison with the computational profile. This is the general trend in all experimental Compton profiles and the reason is believed to lie in the electron-electron correlation effects.[1,5,9,10] The high-momentum components can be seen

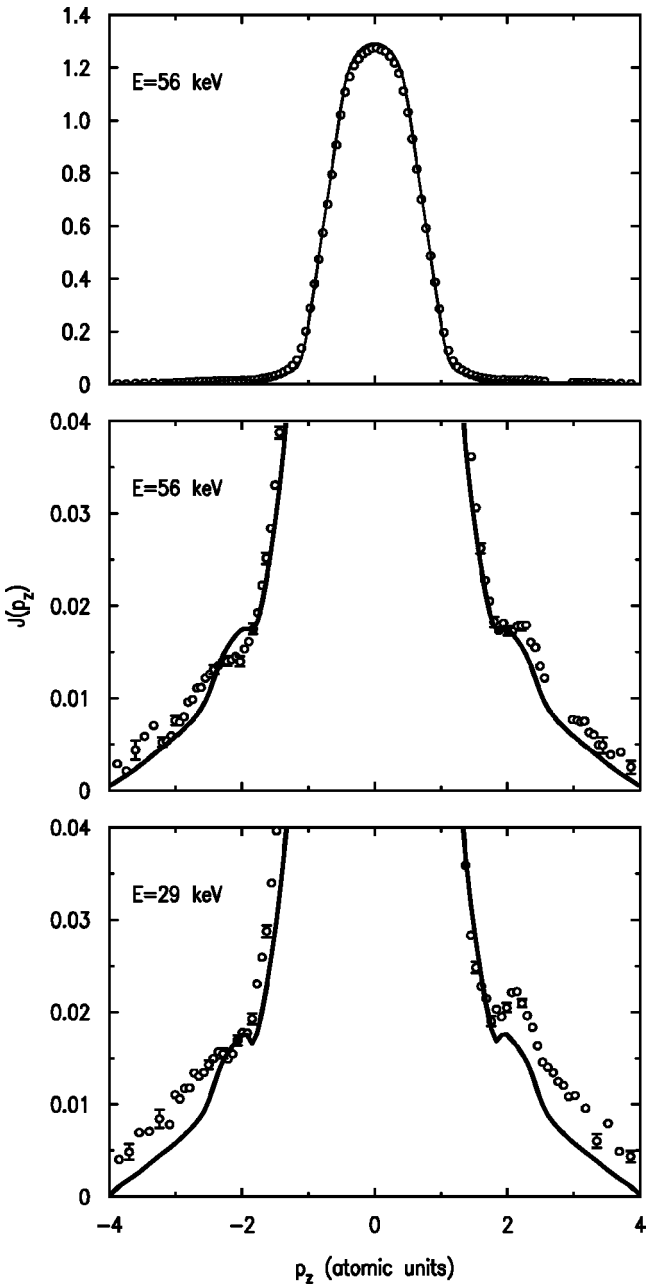

FIG. 1. Top panel: the valence Compton profile of Be along the [110] direction with an incident photon energy of 56 keV. Middle panel: a closeup of the bottom of the same profile as in the top panel. Bottom panel: A closeup of the same valence Compton profile but obtained with an incident photon energy of 29 keV. All data is collected at room temperature. Circles refer to experimental data and the solid line to corresponding pseudopotential-based theoretical Compton profile. The theoretical profile is broadened to reflect the experimental resolution of 0.16 a.u. with an incident photon energy of 56 keV and 0.10 a.u. with an incident photon energy of 29 keV. The error bars are drawn only at every third point for clarity and even then only if they are larger than the symbol size.

as two peaks located at the momenta around $p_z = \pm 2$ a.u. These two distinctive peaks originate from the $\mathbf{G}=[110]$ reciprocal lattice vector, although there are also other lower-lying components that are not as prominent as these two. The intensity of the peaks is quite well reproduced in the computational Compton profiles, but the location is slightly closer to $p_z = 0$ a.u. than is experimentally observed.

It is rather surprising that the shapes of the two peaks in the experimental profiles are slightly different from each other, the one at $+2$ a.u. being quite sharp compared to that at -2 a.u. which is broader and not as prominent. In principle, the momentum density, and thus also the Compton profile, should be symmetric with respect to $p_z = 0$ a.u. and this argument should also hold for the high-momentum components. The reason for the difference in the high-momentum component shapes is not known, and we have not been able to pinpoint any experimental artifact that could explain the observed asymmetry. The fact that the asymmetry is found out to be similar with two different spectrometers, one operating at $E = 56$ keV (Ge440), and one operating at $E = 29$ keV (Si400), rules out most of the possible contamination sources, e.g., fluorescence and glitches of the analyzer crystals being the reason for the asymmetric high-momentum component peaks. Fluorescence contamination is furthermore ruled out, since the multichannel analyzer spectra of both NaI detector and a solid-state Ge detector, which was used as a secondary monitor, did not reveal any fluorescence signals from the sample. A possible spectrometer misalignment cannot be the source since then the asymmetry should be seen in the total Compton profile as well, and not only in the high-momentum component peaks. The symmetry requirement for the Compton profiles is fundamental but only when the ground state of the electron gas is concerned. It is possible that the asymmetry could originate from final-state effects. However, we still do not rule out the possibility of experimental artifacts, although this possibility is believed to be very small. The studies of the origin of the asymmetry are currently under preparation. Nevertheless, the asymmetry should not affect our results on the temperature dependence of the Compton profiles, since the purpose of this work is to study the origin of disagreement between experimental and theoretical Compton profiles of Be seen in Ref. 1.

The temperature dependence of the experimental Compton profiles is presented in Fig. 2, portraying the valence Compton profiles at temperatures 40, 300, 650, and 850 K, zoomed to the bottom region of the Compton profiles. The computational Compton profiles are plotted for comparison in the same figures. At higher temperatures the experimental Compton profiles get narrower, and as their area is always normalized to yield the number of electrons (two in the valence Compton profile of Be), the peak correspondingly gets higher when the temperature rises. This behavior is similar to that observed in Ref. 24. The temperature effect should also be seen as a change in the intensity and the position of the high-momentum components. However, this effect is expected to be much smaller.

In Fig. 3, we present the differences between the Compton profiles measured at different temperatures as a percentage of the valence Compton profile peak height (approximately 1.3

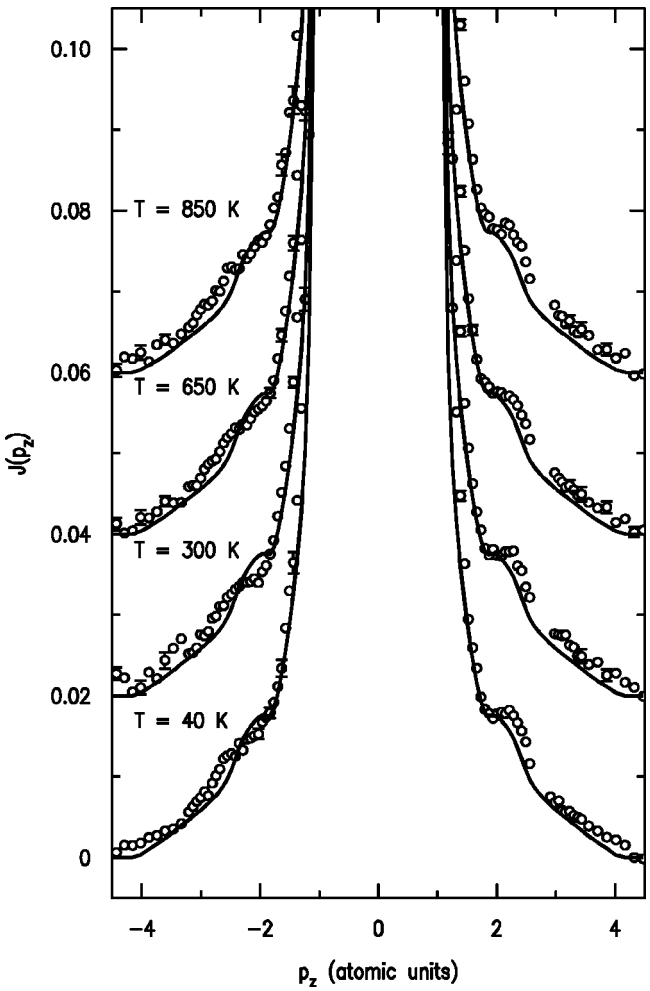

FIG. 2. Circles: the experimental valence Compton profiles of Be along the [110] direction in different sample temperatures obtained at incident photon energy of 56 keV, the momentum resolution begin 0.16 a.u. of momentum. Solid line: the theoretical valence Compton profile calculated for the corresponding temperatures as described in the text. The data sets have been vertically offset by 0.02 electrons/a.u. each for clarity. The error bars are drawn only at every third point for clarity and even then only if they are larger than the symbol size.

electrons/a.u.). The Compton profiles at various temperatures are compared to the data taken at room temperature, since the 40-K data were collected in a different environment than the data at higher temperatures. Each data set is then compared to the room-temperature data collected in the same environment to ensure comparability. The error bars representing statistical uncertainty are plotted only for every third data point for clarity. The corresponding theoretical Compton profile differences are also plotted for comparison; the dashed line depicting theoretical treatment without thermal disorder taken into account and the solid line with thermal disorder. It can be seen that between temperatures of 300 and 40 K the Compton profile (i.e., the electronic structure) of Be does not change significantly, since the difference is barely distinguishable within the statistical accuracy, amounting to less than 0.5% of the valence Compton profile peak height. This is due to the fact that the lattice constants and Debye-

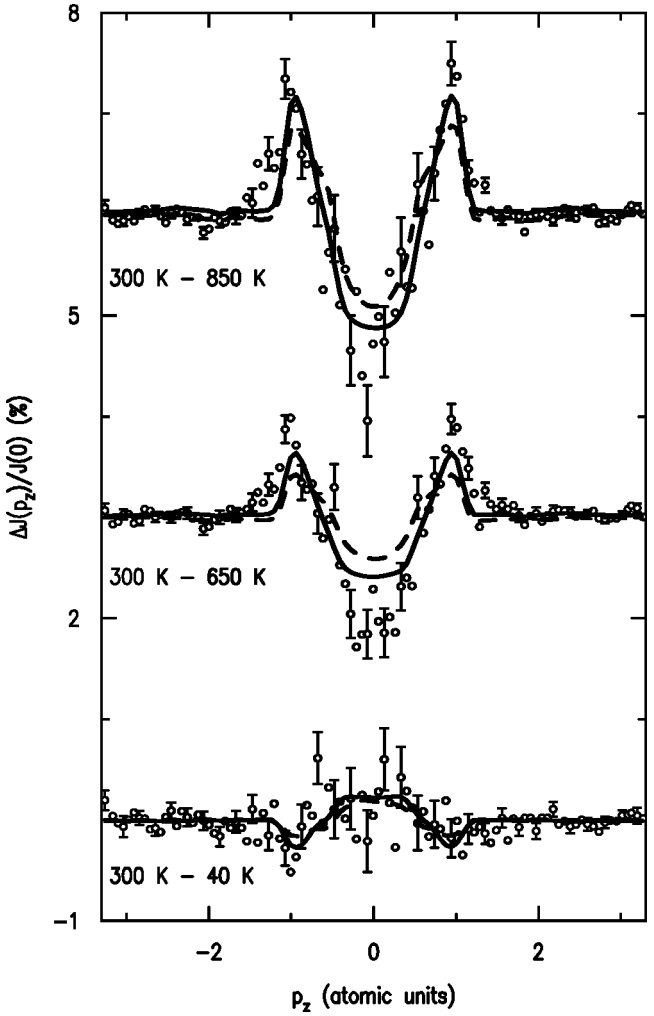

FIG. 3. Circles: differences between experimental Be [110] Compton profiles (presented in Fig. 1) between room temperature and at $T=40$, 650, and 850 K. Solid line: corresponding differences in the pseudopotential-based computed Compton profiles with thermal disorder taken into account. Dashed line: similar theoretical treatment without thermal disorder. The data sets have been vertically offset by 3% units each. The error bars are for clarity drawn only for every third point and even then only if they are larger than the symbol size.

Waller factors for Be change quite slowly below room temperature. The area under each curve is zero since the number of electrons is constant. The overall agreement between experimental and theoretical data is good, but some amount of systematic discrepancy exists in the magnitude of the temperature effect, the experimental differences being slightly larger than the theoretical ones. This is explained by the fact that our empirical local pseudopotential treatment of the wave functions only gives a lower limit for the effect of the finite temperature.

The temperature dependence of the valence electron momentum density of a metal originates from three factors, of which two are of significance in this case, as discussed in Sec. I. First of all, the general behavior of the difference between experimental Compton profiles seen in Fig. 3 is explained by a simple free-electron model. In this model the

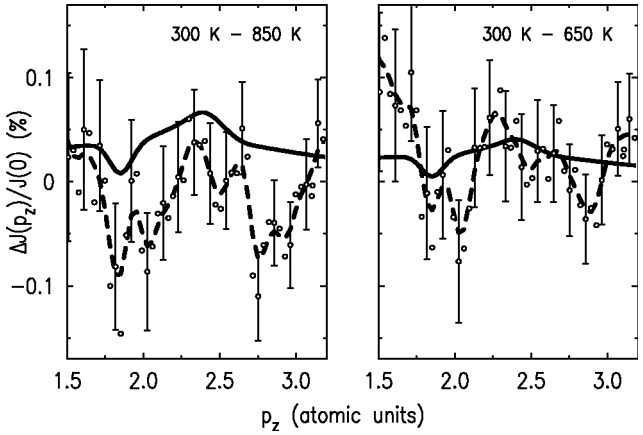

FIG. 4. A closeup of the data in Fig. 3, for Compton profile differences between temperatures of 300–850 K and 300–650 K. Circles represent the experimental data as in Fig. 3, now averaged for $p_z<0$ and $p_z>0$. The error bars are only drawn for every third data point for clarity. The dashed line represents the experimental data smoothed with a Gaussian filter with a FWHM of 0.1 a.u. of momentum (the experimental resolution is 0.16 a.u.) The solid line represents the theoretical difference as calculated by the pseudopotential method taking thermal disorder into account.

only parameter affected by a finite temperature is the Fermi momentum, which gets smaller with increasing temperature as explained in Sec. I. Thus, the Compton profile at a high temperature is narrower than at a low temperature. Similar, but more dramatic effects can be introduced by high pressure, as has recently been demonstrated by Hämäläinen *et al.*[10] Second, when the periodic potential of the ion lattice is taken into account, part of the electron momentum density is transferred away from the first Brillouin zone to the so-called high-momentum components. Their origin can be thought of the electron wave functions being Bragg scattered by the potential. At higher temperatures thermal disorder diminishes this scattering and consequently the intensity of the high-momentum components is lowered. This, in turn, is seen as electron momentum density being more confined in the first Brillouin zone at high temperatures than at low temperatures. This effect has thus the same sign than that of the basic free-electron model. Thus in a real metal, where changes in both the Fermi momentum and the high-momentum components are taken into account, the temperature effect on the momentum density is larger than in the free-electron case.

In addition to this general narrowing of the Compton profile with a raising temperature, the effect of a finite temperature should also be seen on the high-momentum components themselves. These effects would include changes in the position (due to lattice expansion) as well as a diminishing amplitude (due to thermal disorder). The temperature dependence of the high-momentum components is more apparent in the Fig. 4, which shows a zoom-up of the Fig. 3 in the region 1–3 a.u. for the temperature differences between 300, 650, and 850 K. Here the experimental data points with $p_z<0$ a.u. have been averaged with the data points with $p_z>0$ a.u. to improve statistical accuracy. Also in Fig. 4 is plotted the corresponding pseudopotential calculation taking

thermal disorder into account. As seen already in Fig. 3, the Compton profile difference between 300 and 40 K is quite small and is thus not plotted here. The temperature dependence of the high-momentum components is small but just distinguishable within the current statistical accuracy. However, it must be realized that this accuracy is of the order of 0.1% for a single profile at these points. Thus the fact that we actually are able to experimentally resolve this temperature dependence is noteworthy. The important features produced in both the theoretical and experimental data are the dip at 1.9 a.u. and the corresponding peak at 2.4 a.u. The experimentally observed dip at 2.8 a.u. is not reproduced in the theory. This diplike structure is probably due to a high-momentum component corresponding to a higher reciprocal lattice vector that is not accounted for in the theoretical treatment, possibly the $\mathbf{G}=[114]$ vector.

Since the features observed in Fig. 4 are of the order or 0.1% of the total Compton profile peak and barely distinguishable within the statistical accuracy, it is evident that the effect of thermal disorder on the valence electron wave functions does not change significantly within the temperature range studied in this work.

V. SUMMARY AND CONCLUSIONS

The so-called high-momentum components, originating from the electron density centered on reciprocal lattice vectors $\mathbf{G}\neq 0$ in momentum space, were observed directly in a high-resolution Compton scattering experiment using a single-crystal Be sample with two different spectrometer setups operating at incident photon energies of 29 and 56 keV. The measured Compton profiles, including the high-momentum components, were found to be in quite a good agreement with the corresponding pseudopotential-based theoretical Compton profiles, considering that the intensity of the high-momentum components is only 0.5% of the intensity of the total Compton profile. The high statistical accuracy combined with the high resolution of the spectrometer allow us to observe and study the high-momentum components directly. The Compton profiles were measured at various temperatures (40, 300, 650, and 850 K) using an incident photon energy of 56 keV. The temperature dependence of the overall shape of the Be Compton profile was found to be consistent with earlier experiments performed on Li,[9] i.e., the induced changes in the momentum density were dominated by the static lattice expansion. The position and the intensity of the high-momentum component peaks were found to have only minor changes within the utilized temperature range, which confirms that thermal disorder has only a small effect on the periodic lattice modulation of the valence electron wave functions in the case of Be, owing to the relatively high Debye temperature. This means that thermal disorder cannot explain the observed broadening of the high-resolution experimental Compton profiles, in contrary to suggestions of Refs. 17 and 23, and other effects, such as correlation, must be the origin for the observed differences. This study demonstrates that high-resolution Compton-scattering experiments give an excellent opportunity to study the interaction between the valence electrons and the ions comprising a solid metal, as well as thermal disorder in crystalline solids.

ACKNOWLEDGMENTS

We would like to thank Professor Arun Bansil for invaluable discussions. This work was supported by the Academy of Finland (Contract No. 7379/39182/40732) and the German Federal Ministry of Education and Research (Contract No. 05 ST 8 HRA). S.H. is supported by the National Graduate School in Material Physics, funded by the Ministry of Education and the Academy of Finland.

*Electronic address: simo.huotari@helsinki.fi

[1] S. Huotari, K. Hämäläinen, S. Manninen, S. Kaprzyk, A. Bansil, W. Caliebe, T. Buslaps, V. Honkimäki, and P. Suortti, Phys. Rev. B **62**, 7956 (2000).

[2] I. Matsumoto, J. Kwiatkowska, F. Maniawski, A. Bansil, S. Kaprzyk, M. Itou, H. Kawata, and N. Shiotani, J. Phys. Chem. Solids **61**, 375 (2000).

[3] T. Ohata, M. Itou, I. Matsumoto, Y. Sakurai, H. Kawata, N. Shiotani, S. Kaprzyk, P. E. Mijnarends, and A. Bansil, Phys. Rev. B **62**, 16 528 (2000).

[4] K. Hämäläinen, S. Manninen, C.-C. Kao, W. Caliebe, J. B. Hastings, A. Bansil, S. Kaprzyk, and P. M. Platzman, Phys. Rev. B **54**, 5453 (1996).

[5] W. Schülke, G. Stutz, F. Wohlert, and A. Kaprolat, Phys. Rev. B **54**, 14 381 (1996).

[6] S. Manninen, J. Phys. Chem. Solids **61**, 335 (2000).

[7] Y. Sakurai, S. Kaprzyk, A. Bansil, Y. Tanaka, G. Stutz, H. Kawata, and N. Shiotani, J. Phys. Chem. Solids **60**, 905 (1999).

[8] G. Stutz, F. Wohlert, A. Kaprolat, W. Schülke, Y. Sakurai, Y. Tanaka, M. Ito, H. Kawata, N. Shiotani, S. Kaprzyk, and A. Bansil, Phys. Rev. B **60**, 7099 (1999).

[9] C. Sternemann, T. Buslaps, A. Shukla, P. Suortti, G. Döring, and W. Schülke, Phys. Rev. B **63**, 094301 (2001).

[10] K. Hämäläinen, S. Huotari, J. Laukkanen, A. Soininen, S. Manninen, C.-C. Kao, T. Buslaps, and M. Mezouar, Phys. Rev. B **62**, R735 (2000).

[11] M. Itou, Y. Sakurai, T. Ohata, A. Bansil, S. Kaprzyk, Y. Tanaka, H. Kawata, and N. Shiotani, J. Phys. Chem. Solids **59**, 99 (1998).

[12] Y. Sakurai, Y. Tanaka, A. Bansil, S. Kaprzyk, A. T. Stewart, Y. Nagashima, T. Hyodo, S. Nanao, H. Kawata, and N. Shiotani, Phys. Rev. Lett. **74**, 2252 (1995).

[13] C. Blaas, J. Redinger, S. Manninen, V. Honkimäki, K. Hämäläinen, and P. Suortti, Phys. Rev. Lett. **75**, 1984 (1995).

[14] Y. Tanaka, Y. Sakurai, A. T. Stewart, N. Shiotani, P. E. Mijnarends, S. Kaprzyk, and A. Bansil, Phys. Rev. B **63**, 045120 (2001).

[15] L. Oberli, A. A. Manuel, R. Sachot, P. Descouts, M. Peter, L. P. L. M. Rabou, P. E. Mijnarends, T. Hyodo, and A. T. Stewart, Phys. Rev. B **31**, 1147 (1985).

[16] A. A. Manuel, L. Oberli, A. K. Singh, T. Jarlborg, M. Peter, P. E. Mijnarends, L. P. L. M. Rabou, T. Hyodo, and A. T. Stewart, J.

Phys.: Condens. Matter **5**, 8703 (1993).
[17] S. B. Dugdale and T. Jarlborg, Solid State Commun. **105**, 283 (1998).
[18] C. Keffer, T. M. Hayes, and A. Bienenstock, Phys. Rev. Lett. **21**, 1676 (1968).
[19] C. Sternemann, K. Hämäläinen, A. Kaprolat, A. Soininen, G. Döring, C.-C. Kao, S. Manninen, and W. Schülke, Phys. Rev. B **62**, R7687 (2000).
[20] J. Soininen, K. Hämäläinen, and S. Manninen, Phys. Rev. B **64**, 125116 (2001).
[21] S. Huotari, K. Hämäläinen, S. Manninen, M. Marangolo, and A. Issolah, J. Phys. Chem. Solids **62**, 2205 (2001).
[22] L. Lam and P. Platzman, Phys. Rev. B **9**, 5122 (1974).
[23] C. Filippi and D. M. Ceperley, Phys. Rev. B **59**, 7907 (1999).
[24] C. Sternemann, G. Döring, C. Wittkop, W. Schülke, A. Shukla, T. Buslaps, and P. Suortti, J. Phys. Chem. Solids **61**, 379 (2000).
[25] K. J. Chen, V. Caspar, C. Bellin, and G. Loupias, Solid State Commun. **110**, 357 (1999).
[26] B. I. Lundqvist and C. Lydén, Phys. Rev. B **4**, 3360 (1971).
[27] W. A. Pickett, Comput. Phys. Rep. **9**, 115 (1989).
[28] W. Schülke, U. Bonse, H. Nagasawa, S. Mourikis, and A. Kaprolat, Phys. Rev. Lett. **59**, 1361 (1987).
[29] L.-M. Peng, G. Ren, S. L. Dudarev, and M. J. Whelan, Acta Crystallogr., Sect. A: Found. Crystallogr. **52**, 456 (1996).
[30] B. Eisenmann and H. Schäfer, in *Numerical Data and Functional Relationships in Science and Technology*, Landolt and Börnstein, New Series, Group III, Vol. 14a (Springer, New York, 1988), p. 406, only lattice constants at temperatures down to 100 K were recorded so the 40 K lattice constants were obtained by extrapolation.
[31] P. Suortti, T. Buslaps, P. Fajardo, V. Honkimäki, M. Kretzschmer, U. Lienert, J. E. McCarthy, M. Renier, A. Shukla, T. Tschentscher *et al.*, J. Synchrotron Radiat. **6**, 69 (1999).